

Chapter 1

Video Gallery of Flow Phenomena

(This chapter was updated in 2007. *Note: the new videos require use of an updated video player.*)

Summary: Numerous videos have been assembled here for two-phase flows and heat transfer phenomena (and still more will be added in the future) and are available here for the reader to view. Presently, only two-phase videos are shown but videos of single-phase enhancement phenomena will be included in the future.

1.1 INTRODUCTION TO THE VIDEO GALLERY

The motive behind the preparation of this video gallery is to make videos of single-phase and two-phase flow and heat transfer phenomena available for general viewing. For thermal designers normally performing computer calculations on heat exchangers, this is an opportunity for them to actually see what some of the processes really look like, albeit in idealized test conditions. The idea is also to make this chapter a forum to display interesting videos of such phenomena for others to see.

Note: Since the original video files are typically too large (5-40 Megabits) to view directly via the internet, the videos shown have had to cut to short time sequences (typically 2 seconds or less) that are looped to give the sensation of a continuous process and also processing of the images has been applied to achieve smaller file sizes, but at a small lose of quality. Some patience may be required on behalf of the reader to view these video files via the Internet.

To use this chapter: The chapter is organized by type of flow. Within each section, videos are listed by the flow process they show; the reader needs only to click on the video of his choice on the list to see the video and also obtain a brief description of the test setup and experimental conditions.

1.2 TWO-PHASE FLOW PATTERNS IN HORIZONTAL TUBES

Figure 1.1 depicts a two-phase flow pattern map for flow in a horizontal tube, illustrating the types of two-phase flow patterns typical of these flows and the range of conditions where particular flow regimes occur. Within a horizontal evaporator tube, Figure 1.2 depicts a composite diagram of the flow patterns that may be encountered when going from a subcooled liquid to complete evaporation. Similarly, Figure 1.3 shows composite diagrams of flow patterns confronted in condensation at high and low flow rates. The videos in this section, listed below, show numerous examples of these flows.

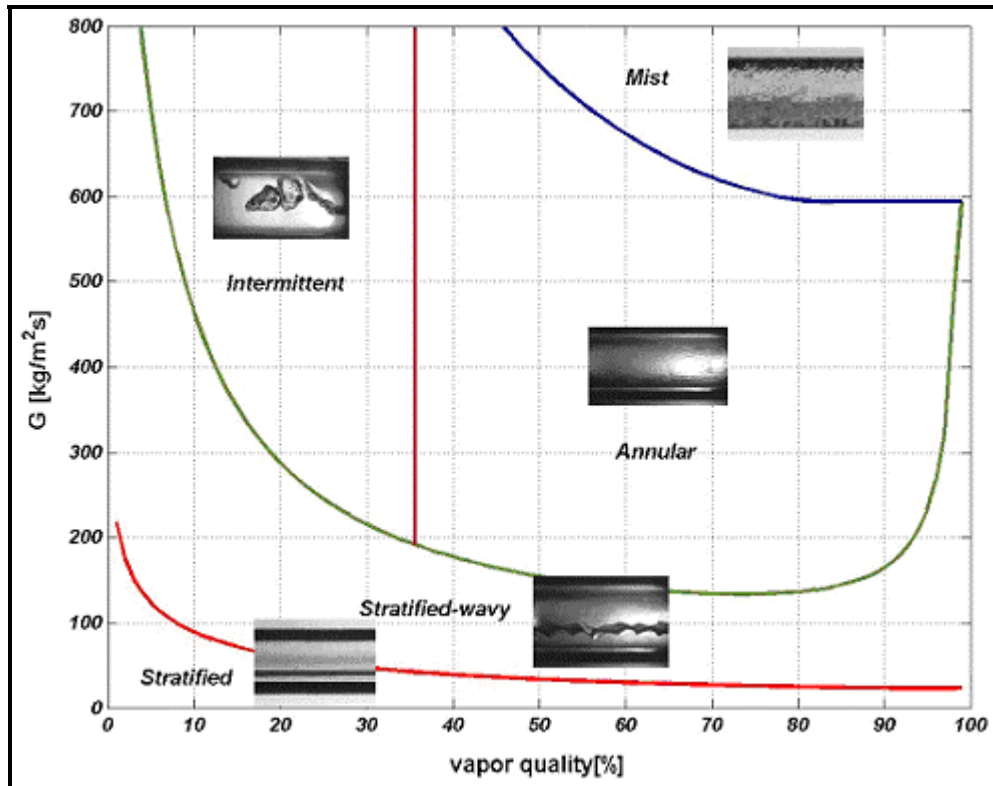


Figure 1.1. Flow pattern map for R-22 at a saturation temperature of 5°C (41°F) showing transition boundaries between two-phase flow regimes [where G is the mass velocity of the liquid + vapor inside the cross-section of the tube of internal diameter $d = 13.82$ mm (0.544 in.)].

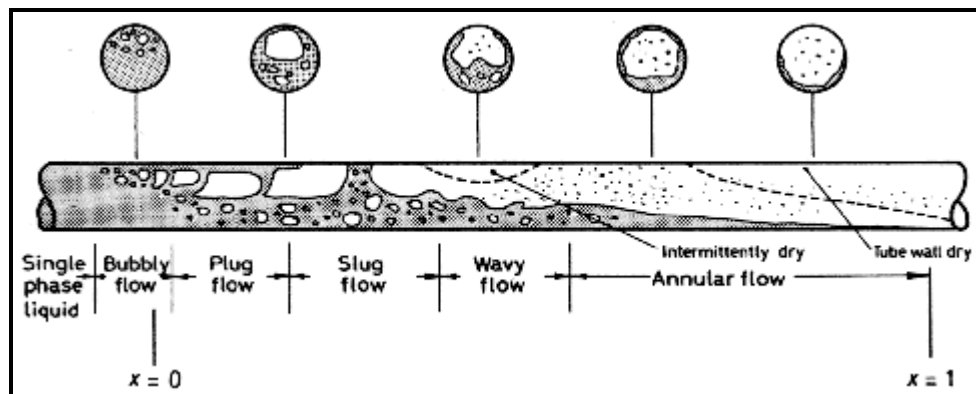


Figure 1.2. Illustration of two-phase flow patterns occurring in horizontal evaporator tube.

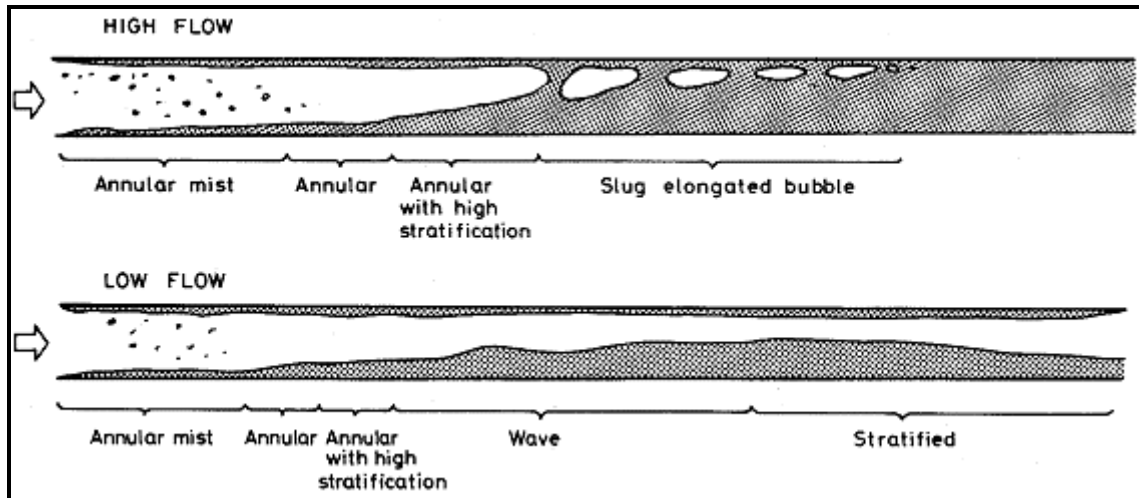


Figure 1.3. Illustration of two-phase flow patterns occurring in horizontal condenser tubes.

List of videos: (click on the one you wish to see)

Video 1.2.1: Bubble flow. The video displays flow of isolated bubbles inside a horizontal sightglass of 14.0 mm (0.551 in.) internal diameter. This flow is at a moderate mass velocity at a very low vapor quality and the bubble is essentially the initial step towards arriving at a plug flow. The fluid is ammonia at 5°C (41°F). The video was taken by Dr. O. Zürcher in collaboration with Profs. J.R. Thome and D. Favrat at the Swiss Federal Institute of Technology Lausanne (EPFL). For a description of the test facility, refer to: Zürcher, Favrat and Thome (2002).

Video 1.2.2: Stratified-wavy flow. The video displays a stratified-wavy flow (liquid in bottom and vapor in top of tube) inside a horizontal sightglass of 14.0 mm (0.551 in.) internal diameter. The fluid is ammonia at 5°C (41°F), a vapor quality of 0.20 and mass velocity of 26 kg/m²s (19126 lb/hr ft²). The video was taken by Dr. O. Zürcher in collaboration with Profs. J.R. Thome and D. Favrat at the Swiss Federal Institute of Technology Lausanne (EPFL). For a description of the test facility, refer to: Zürcher, Favrat and Thome (2002).

Video 1.2.3: Plug/slug to intermittent flow transition. The video displays a plug/slug flow at relatively low vapor quality inside a horizontal sightglass of 14.0 mm (0.551 in.) internal diameter. The fluid is ammonia at 5°C (41°F), a vapor quality of 0.06 and mass velocity of 180 kg/m²s (132408 lb/hr ft²). The video was taken by Dr. O. Zürcher in collaboration with Profs. J.R. Thome and D. Favrat at the Swiss Federal Institute of Technology Lausanne (EPFL). For a description of the test facility, refer to: Zürcher, Favrat and Thome (2002).

Video 1.2.4: Annular flow. The video displays an annular flow (liquid in an annular film on tube perimeter and vapor in center of tube) at relatively high vapor quality inside a horizontal sightglass of 14.0 mm (0.551 in.) internal diameter. The fluid is ammonia at 5°C (41°F), a vapor quality of 0.80 and mass velocity of 122 kg/m²s (89743 lb/hr ft²). The video was taken by Dr. O. Zürcher in collaboration with Profs. J.R. Thome and D. Favrat at the Swiss Federal Institute of Technology Lausanne (EPFL). For a description of the test facility, refer to: Zürcher, Favrat and Thome (2002).

Video 1.2.5: Annular flow with partial dryout. The video displays an annular flow with partial dryout around the upper perimeter (liquid in bottom and vapor in top of tube) at relatively high vapor quality (*essentially a stratified-wavy flow created by the partial dryout around upper perimeter of the tube*)

inside a horizontal sightglass of 14.0 mm (0.551 in.) internal diameter. The fluid is ammonia at 5°C (41°F), a vapor quality of 0.80 and mass velocity of 41 kg/m²s (30160 lb/hr ft²). The video was taken by Dr. O. Zürcher in collaboration with Profs. J.R. Thome and D. Favrat at the Swiss Federal Institute of Technology Lausanne (EPFL). For a description of the test facility, refer to: Zürcher, Favrat and Thome (2002).

Video 1.2.6: Condensation flow regimes in plain tube. The video displays the exit of a horizontal condenser tube cut at a 45° degree angle and situated inside a viewing chamber. The view is from the side. First, a flow pattern map is shown illustrating two superficial vapor velocities, J_G , that were studied, plotted versus the Martinelli parameter, X_{tt} . The inside diameter of the tube is 8.0 mm (0.315 in.). The fluid is R-134a at 40°C (104°F), vapor qualities (x) of 0.49 and 0.26, and mass velocities (G) of 200 and 400 kg/m²s (147120 and 294240 lb/hr ft²). The video was taken under the direction of Prof. Alberto Cavallini at the University of Padova, Padova, Italy. For a description of their test facility and related investigation, refer to: Censi et al. (2003). For a description of their flow pattern map, refer to: Cavallini et al. (2002).

Video 1.2.7: Condensation flow regimes in microfin tube. The video displays the exit of a horizontal condenser tube cut at a 45° degree angle and situated inside a viewing chamber. The view is from the side. First, a flow pattern map is shown illustrating two superficial vapor velocities, J_G , that were tested plotted versus the Martinelli parameter, X_{tt} . The inside diameter at the fin tip is 7.69 mm (0.303 in.). The fluid is R-134a at 40°C (104°F), vapor qualities (x) of 0.51 and 0.25, and mass velocities (G) of 200 and 400 kg/m²s (147120 and 294240 lb/hr ft²). This video can be compared to the plain tube video 1.2.6 and it is seen that the microfins imposed a more uniform distribution of liquid around the tube perimeter, especially at the lower mass velocity. The video was taken under the direction of Prof. Alberto Cavallini at the University of Padova, Padova, Italy. For a description of their test facility and related investigation, refer to: Censi et al. (2003). For a description of their flow pattern map, refer to: Cavallini et al. (2002).

Video 1.2.8: Annular flow with entrainment of liquid droplets. The video displays a side view of annular flow with a large number of small liquid droplets in a high velocity vapor core of the flow, inside a horizontal sightglass of 13.6 mm (0.535 in.) internal diameter. The fluid is R-22 at 5°C (41°F), a vapor quality of 0.65 and mass velocity of 600 kg/m²s (441000 lb/hr ft²). The video was taken by L. Wojtan in collaboration with Prof. J.R. Thome at the Swiss Federal Institute of Technology Lausanne (EPFL). For a description of the test facility, refer to: Ursenbacher, Wojtan and Thome (2004) and Wojtan, Ursenbacher and Thome (2004).

Video 1.2.9: Transition from annular to mist flow. The video displays a side view of a flow in the transition regime between annular flow with liquid entrainment (lower portion of tube) and mist flow (upper portion of tube), inside a horizontal sightglass of 13.6 mm (0.535 in.) internal diameter. The fluid is R-22 at 5°C (41°F), a vapor quality of 0.79 and mass velocity of 500 kg/m²s (367500 lb/hr ft²). The video was taken by L. Wojtan in collaboration with Prof. J.R. Thome at the Swiss Federal Institute of Technology Lausanne (EPFL). For a description of the test facility, refer to: Ursenbacher, Wojtan and Thome (2004) and Wojtan, Ursenbacher and Thome (2004).

Video 1.2.10: Mist flow. The video displays a cross-sectional view of mist flow (small liquid droplets in a high velocity vapor flow) inside a horizontal sightglass of 13.6 mm (0.535 in.) internal diameter. The fluid is R-22 at 5°C (41°F), a vapor quality of 0.90 and mass velocity of 400 kg/m²s (294000 lb/hr ft²). The cross-section of the tube is illuminated by a laser sheet and the liquid is highlighted by a trace of fluorescent powder. The video was taken by L. Wojtan in collaboration with Prof. J.R. Thome and Dr. T. Ursenbacher at the Swiss Federal Institute of Technology Lausanne (EPFL). For a description of the test facility, refer to: Ursenbacher, Wojtan and Thome (2004) and Wojtan, Ursenbacher and Thome (2004).

Video 1.2.11: *Annular flow with twisted tape insert at low mass velocity.* The video displays an annular flow with swirl from a twisted tape for flow inside a horizontal sight glass of 8.0 mm (0.315 in.) internal diameter. The fluid is R-507A at 5°C (41°F), a vapor quality of 0.33 and mass velocity of 100 kg/m²s (73500 lb/hr ft²). In a plain tube without twisted tape, the flow would be stratified-wavy and it is clear that the tape converts the flow to annular flow, including some liquid entrainment. The video was taken by J. Moreno Quiben in collaboration with Prof. J.R. Thome at the Swiss Federal Institute of Technology Lausanne (EPFL). For a description of the test facility (*without the twisted tape*), refer to: Moreno Quibén and Thome (2003).

Video 1.2.12: *Annular flow with twisted tape insert at medium mass velocity.* The video displays an annular flow with swirl from a twisted tape for flow inside a horizontal sight glass of 8.0 mm (0.315 in.) internal diameter. The fluid is R-507A at 5°C (41°F), a vapor quality of 0.18 and mass velocity of 150 kg/m²s (147100 lb/hr ft²). The flow is annular with a swirl effect from the tape and some liquid entrainment. The video was taken by J. Moreno Quiben in collaboration with Prof. J.R. Thome at the Swiss Federal Institute of Technology Lausanne (EPFL). For a description of the test facility (*without the twisted tape*), refer to: Moreno Quibén and Thome (2003).

Video 1.2.13: *Annular flow with twisted tape insert at high mass velocity.* The video displays an annular flow with swirl from a twisted tape for flow inside a horizontal sight glass of 8.0 mm (0.315 in.) internal diameter. The fluid is R-507A at 5°C (41°F), a vapor quality of 0.20 and mass velocity of 300 kg/m²s (220500 lb/hr ft²). The flow is annular with a swirl effect from the tape and some liquid entrainment. The video was taken by J. Moreno Quiben in collaboration with Prof. J.R. Thome at the Swiss Federal Institute of Technology Lausanne (EPFL). For a description of the test facility (*without the twisted tape*), refer to: Moreno Quibén and Thome (2003).

A study on air-water flow patterns inside a horizontal clear polycarbonate tube of 25.4 mm (1.0 in.) internal diameter was undertaken with water and air at about 15°C (60°F). The videos were taken by Jae-yong Kim in collaboration with Prof. Afshin Ghajar at the School of Mechanical and Aerospace Engineering, Oklahoma State University. For a description of their test facility, refer to Ghajar and Tang (2007).

Video 1.2.14: *Flow patterns in a horizontal tube as a function of gas superficial Reynolds number.* The tests were done for a fixed value of $Re_{SL} = 5000$ (the liquid superficial Reynolds number) and a range of $Re_{SG} = 1500$ to 47600 (the gas superficial Reynolds number). The superficial Reynolds number is that for a particular phase (its fraction of the total flow) as if it was flowing alone in the entire cross-section of the channel. Notice in particular the wide transition range between the different flow patterns. Initially the flow is in the slug flow pattern ($Re_{SL} = 1500$ to 6000), whereas for $Re_{SL} > 6000$ the flow is considered slug-wavy while for $Re_{SL} > 16000$ turns into wavy-annular and finally becomes purely annular flow for $Re_{SL} > 32000$.

Video 1.2.15: *Annular flow in horizontal and slightly inclined tubes.* The tests were done for inclination angles of 0°, 2°, 5° and 7° with respect to the horizontal. In the video, the liquid superficial Reynolds number (Re_{SL}) is fixed at 5000 and the gas superficial Reynolds number (Re_{SG}) is kept at 47600. Notice in particular that there is no distinct effect on the flow movement due to inclination observable for the annular flow (this is in sharp contrast to what is observed for slug flow – refer to Video 1.2.16). The reason being, the inertia force carried by the flow of air in an annular flow is much larger than the buoyancy force difference between the air and water, such that there is almost no change in the shape of the annular flow pattern due to small angles of inclination.

Video 1.2.16: *Slug flow in horizontal and slightly inclined tubes.* The tests were done for inclination angles of 0°, 2°, 5° and 7° from the horizontal. In the video, the liquid superficial Reynolds number

(Re_{SL}) is fixed at 5000 and the gas superficial Reynolds number (Re_{SG}) is kept at 1500. Notice in particular that at the 2° inclination angle not all the bubbles in the flow stay stationary in comparison to the bubbles in the horizontal flow. For the 5° and 7° inclination angles, the slugs start moving backward (back flow). The reason being, as the tube is inclined, the balance between the inertia force and buoyancy force is changed and rebalanced, such that the increase of the buoyancy force of the air affects the turbulence and the speed of the slug's traverse. In contrast to the annular flow video (see Video 1.2.15), inclination does show a significant influence on the slug flow movement.

A new, novel technique to highlight two-phase flow patterns in horizontal tubes has been proposed by Jassim, Newell and Chato (2007), from the Jassim (2006) thesis, for image enhancement and as an image recognition aid for determining flow regimes to develop probabilistic two-phase flow regime maps. The tests were for R-134a and R-410A with adiabatic horizontal flow at a saturation temperature of 25°C (77°F). In their videos, back lighting of the tube through a paper with black lines was used to highlight the liquid-vapor interface and the liquid phase as shown in Figure 1.4.

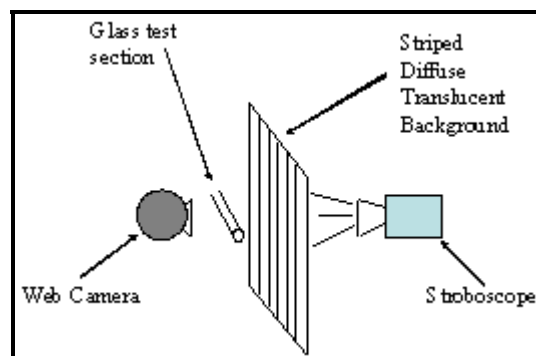


Figure 1.4. Back lighting set up of Jassim (2006) to apply black lines onto the video images.

The videos were taken for four glass tube internal diameters: 8.00 mm (0.315 in.), 5.43 mm (0.214 in.), 3.90 mm (0.154 in.) and 1.74 mm (0.068 in.). The videos were taken by E.W. Jassim during his Ph.D. in the laboratory of Profs. T.A. Newell and J.C. Chato at the Air Conditioning and Refrigeration Center at the Department of Mechanical Science and Engineering at the University of Illinois at Urbana-Champaign. The test setup and results are described in Jassim's (2006) thesis and in Jassim, Newell and Chato (2007). For detailed descriptions of the plates and their dimensions, refer to the thesis or paper.

Video 1.2.17: *Two-phase flow of R-134a in a 1.7 mm tube (1st run).* This run is for a mass velocity of $400 \text{ kg/m}^2\text{s}$ (294000 lb/hft^2) at a vapor quality of 2% showing a slug flow.

Video 1.2.18: *Two-phase flow of R-134a in a 1.7 mm tube (2nd run).* This run is for a mass velocity of $400 \text{ kg/m}^2\text{s}$ (294000 lb/hft^2) at a vapor quality of 8% showing a slug flow.

Video 1.2.19: *Two-phase flow of R-134a in a 1.7 mm tube (3rd run).* This run is for a mass velocity of $400 \text{ kg/m}^2\text{s}$ (294000 lb/hft^2) at a vapor quality of 99% showing an annular flow.

Video 1.2.20: *Two-phase flow of R-134a in a 3.9 mm tube (1st run).* This run is for a mass velocity of $100 \text{ kg/m}^2\text{s}$ (73600 lb/hft^2) at a vapor quality of 4% showing a slug flow.

Video 1.2.21: *Two-phase flow of R-134a in a 3.9 mm tube (2nd run).* This run is for a mass velocity of $200 \text{ kg/m}^2\text{s}$ (147000 lb/hft^2) at a vapor quality of 12% showing an intermittent flow.

Video 1.2.22: *Two-phase flow of R-134a in a 5.4 mm tube (1st run).* This run is for a mass velocity of 100 kg/m²s (73600 lb/hft²) at a vapor quality of 12% showing a slug/stratified-wavy flow regime.

Video 1.2.23: *Two-phase flow of R-134a in a 5.4 mm tube (2nd run).* This run is for a mass velocity of 200 kg/m²s (147000 lb/hft²) at a vapor quality of 3% showing a slug flow regime.

Video 1.2.24: *Two-phase flow of R-134a in a 5.4 mm tube (3rd run).* This run is for a mass velocity of 200 kg/m²s (147000 lb/hft²) at a vapor quality of 39% showing an annular flow regime.

Video 1.2.25: *Two-phase flow of R-410A in a 1.7 mm tube (1st run).* This run is for a mass velocity of 400 kg/m²s (294000 lb/hft²) at a vapor quality of 44% showing an annular flow.

Video 1.2.26: *Two-phase flow of R-410A in a 3.9 mm tube (1st run).* This run is for a mass velocity of 300 kg/m²s (221000 lb/hft²) at a vapor quality of 55% showing an annular flow.

Video 1.2.27: *Two-phase flow of R-410A in a 3.9 mm tube (2nd run).* This run is for a mass velocity of 400 kg/m²s (294000 lb/hft²) at a vapor quality of 6% showing a slug flow.

Video 1.2.28: *Two-phase flow of R-410A in a 5.4 mm tube (1st run).* This run is for a mass velocity of 100 kg/m²s (73600 lb/hft²) at a vapor quality of 7% showing a slug flow.

Video 1.2.29: *Two-phase flow of R-410A in a 5.4 mm tube (2nd run).* This run is for a mass velocity of 400 kg/m²s (294000 lb/hft²) at a vapor quality of 18% showing an intermittent/annular flow.

Video 1.2.30: *Two-phase flow of R-410A in a 5.4 mm tube (3rd run).* This run is for a mass velocity of 400 kg/m²s (294000 lb/hft²) at a vapor quality of 87% showing an annular flow.

Numerous horizontal two-phase flow visualization studies have been undertaken at the UKAEA Harwell Laboratory under the direction of Prof. G. Hewitt of Imperial College, London. A selection of videos provided by Prof. Hewitt is shown below. For a description of his earlier work on two-phase flow visualization, refer to Arnold and Hewitt (1967) and Hewitt and Whalley (1980).

Video 1.2.31: *Axial view of annular flow in a horizontal tube.* The video shows an axial view taken of annular flow in a horizontal tube. The tests were done with water and air with the camera mounted at the end of the test section looking upstream in the tube with a flash tube synchronized with the camera for illumination of the flow from the side of the tube. The large fraction of the liquid phase entrained in the central vapor core is clearly visible. The video was taken at UKAEA Harwell Laboratory under direction of Prof. G. Hewitt of Imperial College London.

Video 1.2.32: *Axial view of annular air-water flow in a large horizontal tube.* The video shows an axial view taken of annular flow in a 78 mm (3.07 in.) horizontal tube. The tests were done with water and air with the camera mounted as shown in Figure 1.5. At the location of the “eye” looking upstream in the tube with a view of the flow at the illuminated plane. The air velocity was 20 m/s (65.6 ft/s) and the water velocity was 0.002 m/s (0.066 ft/s).

The large amount of the liquid phase entrained in the central vapor core is clearly visible, erupting from the thicker layer at the bottom of the tube. For a description of the test facility, see Badie, Lawrence and Hewitt (2001).

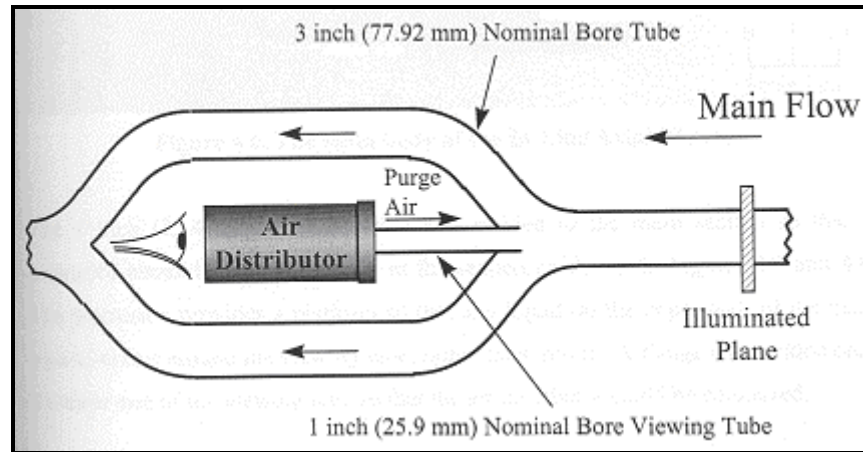


Figure 1.5. Diagram of visualization test section of Badie, Lawrence and Hewitt ((2001).

Video 1.2.33: *Axial view of annular air-oil flow in a large horizontal tube.* The video shows an axial view taken of annular flow in the 78 mm (3.07 in.) horizontal tube described above. The tests were done with oil and air. The air velocity was 20 m/s (65.6 ft/s) and the oil velocity was 0.02 m/s (0.066 ft/s). The large fraction of the liquid phase entrained in the central vapor core is clearly visible, erupting from the thicker layer at the bottom of the tube and then draining back to the bottom. The video was taken by Mr. Sharokh Badie under the direction of Prof. G. Hewitt. For a description of the test facility, refer to: Badie, Lawrence and Hewitt (2001).

Video 1.2.34 and video 1.2.35: *Axial views of flow in a horizontal coiled tube.* The videos show axial views taken of flow in a horizontal coiled tube. The tests were done with water and air. The top video shows the flow traveling mostly on the inside of the curved surface and the lower video shows the flow after inversion with more liquid on the outside of the curved surface of the coil. The videos were taken by Prof. G. Hewitt at the Harwell Laboratory in the 1960's. The inversion effect was analyzed by Hewitt and Jayanti (1992) who explained it in terms of a balance of centrifugal, pressure and circumferential shear stress forces.

1.3 VOID FRACTION MEASUREMENTS IN HORIZONTAL TUBES

Dynamic cross-sectional void fractions have been measured at the Laboratory of Heat and Mass Transfer (LTCM) at the Swiss Federal Institute of Technology Lausanne (EPFL). In Figure 1.6 the simplified diagram of the experimental visualization setup is shown where the two-phase refrigerant flows inside the horizontal tube and is viewed from an oblique angle through the glass tube wall by the camera. The effects refraction through the glass tube wall and oblique view of the flow cross-section by the camera objective are taken into account in reconstruction of the true image, such that the flow structure can be analyzed as described in Figure 1.7 For a complete description, refer to: Ursenbacher, Wojtan and Thome (2004) and Wojtan, Ursenbacher and Thome (2004).

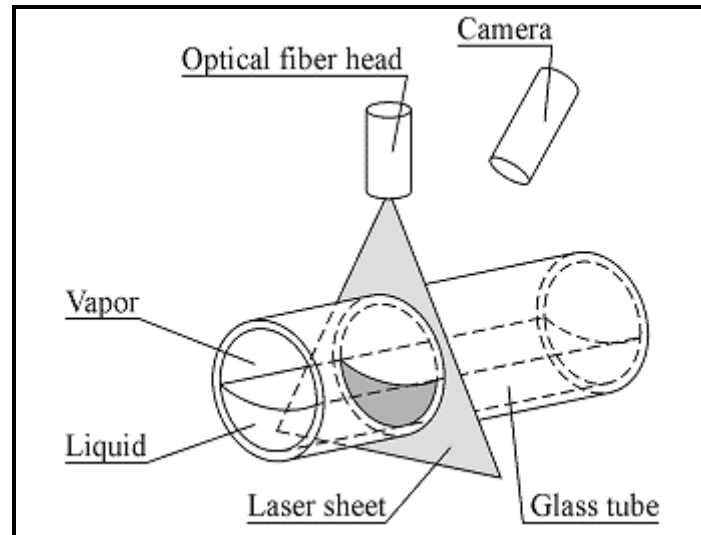


Figure 1.6. Cross-sectional void fraction visualization setup for a stratified flow in a horizontal tube.

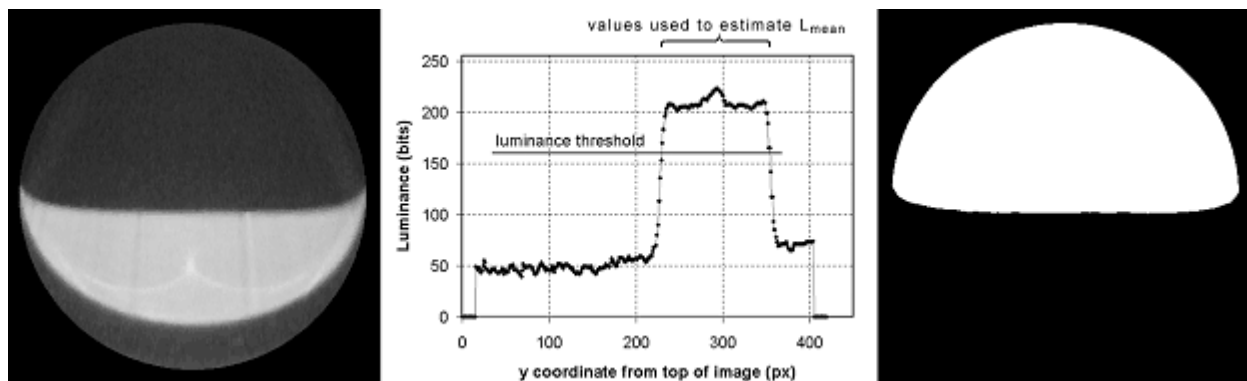


Figure 1.7. Left: Transformed cross-sectional image from actual video image of flow; Middle: variation in luminance intensity along the center vertical line of image; Right: Detected vapor (white) and liquid (black) zones in the tube, depicting shape of interface, dry angle around upper perimeter of tube and dynamic void fraction, i.e. number of white pixels divided by number of all white and black pixels.

List of videos: (click on the one you wish to see)

[Video 1.3.1: Overall view of air-water test facility with a slug flow.](#) The video shows the LTCM air-water test facility for observing two-phase flows and measuring void fractions inside a horizontal sight glass of 13.8 mm (0.543 in.) internal diameter. The liquid is water and the gas is air at room temperature. The video was taken in Laboratory of Heat and Mass Transfer under the direction of Prof. J.R. Thome at the Swiss Federal Institute of Technology Lausanne (EPFL).

[Video 1.3.2: Close up of air-water loop showing the video camera with a slug flow.](#) The video shows LTCM test facility for observing two-phase flows and measuring void fractions inside a horizontal sight glass of 13.8 mm (0.543 in.) internal diameter. The video shows the placement of the video camera above the glass tube for taking void fraction videos. The liquid is water and the gas is air at room temperature. The video was taken in Laboratory of Heat and Mass Transfer under the direction of Prof. J.R. Thome at the Swiss Federal Institute of Technology Lausanne (EPFL).

Video 1.3.3: *Air-water test loop with laser sheet cutting across tube just below camera.* The video shows a vertical laser sheet cutting across a horizontal tube for a slug flow inside a horizontal sightglass of 13.8 mm (0.543 in.) internal diameter. The video camera for recording the cross-section of the flow at the laser sheet is located just above and to the right of the images to be recorded. The second tube is only there for some other preliminary tests. The liquid is water and the gas is air at room temperature. The video was taken in Laboratory of Heat and Mass Transfer (LTCM) under the direction of Prof. J.R. Thome at the Swiss Federal Institute of Technology Lausanne (EPFL).

Video 1.3.4: *Original video of slug flow with effects of refractions of light.* The video shows the original view image (in slow motion) of the cross-section of the two-phase flow inside a horizontal sightglass of 13.8 mm (0.543 in.) internal diameter with the cross-sectional image compressed and distorted by the angle of the camera and the refraction of light through the glass tube wall. The liquid is water and the gas is air at room temperature. The video was taken in Laboratory of Heat and Mass Transfer by L. Wojtan under the direction of Prof. J.R. Thome at the Swiss Federal Institute of Technology Lausanne (EPFL). The video is not at actual speed.

Video 1.3.5: *Transformed video of same slug flow video.* The video shows the corrected video image (slow motion) of Video 1.3.4 in black and white inside a horizontal sightglass of 13.8 mm (0.543 in.) internal diameter, showing the cross-sectional view of the flow. The liquid is water (white) and the gas (black) is air at room temperature. The black areas *below* the liquid interface are caused by reflections and do not represent gas. The video was processed in Laboratory of Heat and Mass Transfer (LTCM) by Dr. T. Ursenbacher under the direction of Prof. J.R. Thome at the Swiss Federal Institute of Technology Lausanne (EPFL). The video is not at actual speed.

Video 1.3.6: *Black-and-white version of transformed image of same slug flow video.* The video shows the digitized image (slow motion) of a slug flow inside a horizontal sightglass of 13.8 mm internal diameter. The liquid occupies the lower portion of the tube (black) and the vapor the upper portion of the tube (white). The number of white pixels divided by the total pixels of the tube cross-section gives the instantaneous void fraction for each video image. The dry angle around the upper perimeter of the tube changes during the flow. The liquid is water and the gas is air at room temperature. The video was processed in the Laboratory of Heat and Mass Transfer (LTCM) by Dr. T. Ursenbacher under the direction of Prof. J.R. Thome at the Swiss Federal Institute of Technology Lausanne (EPFL). The video is not at actual speed.

Video 1.3.7: *R-410A slug flow video showing measured interfacial contour.* The video shows the digitized image of a slug flow inside a horizontal sightglass of 13.6 mm (0.535 in.) internal diameter. The liquid occupies the lower portion of the tube (white) and the vapor the upper portion of the tube (gray). The interface contour detected by the image processing program is superimposed on each image. The number of pixels above the interfacial contour divided by the total pixels of the tube cross-section gives the instantaneous void fraction for each video image. The dry angle around the upper perimeter of the tube is evident and changes during the flow. When liquid slugs pass by, the total cross-section is occupied by liquid. The fluid is R-410A at 5°C (41°F), a vapor quality of 0.103 and a mass velocity of 150 kg/m²s (110340 lb/hr ft²). The video was obtained and processed in the Laboratory of Heat and Mass Transfer (LTCM) by L. Wojtan and Dr. T. Ursenbacher under the direction of Prof. J.R. Thome at the Swiss Federal Institute of Technology Lausanne (EPFL). The video is at actual speed. The work is described in Ursenbacher, Wojtan and Thome (2004).

Video 1.3.8: *R-410A stratified-wavy flow video showing measured interfacial contour.* The video shows the digitized image of a stratified-wavy flow inside a horizontal sightglass of 13.6 mm (0.535 in.) internal diameter. The liquid occupies the lower portion of the tube (white) and the vapor the upper portion of the

tube (gray). The interface contour detected by the image processing program is superimposed on each image. The number of pixels above the interfacial contour divided by the total pixels of the tube cross-section gives the instantaneous void fraction for each video image. The dry angle around the upper perimeter of the tube is evident and changes during the flow. The movement of the contour with time is the result of the interfacial waves created by the vapour shear of the vapor on the liquid. The fluid is R-410A at 5°C (41°F), a vapour quality of 0.20 and a mass velocity of 70 kg/m²s (51492 lb/hr ft²). The video was obtained and processed in the Laboratory of Heat and Mass Transfer (LTCM) by L. Wojtan and Dr. T. Ursenbacher under the direction of Prof. J.R. Thome at the Swiss Federal Institute of Technology Lausanne (EPFL). The video is at actual speed. The work is described in Ursenbacher, Wojtan and Thome (2004).

1.4 TWO-PHASE FLOW PATTERNS IN VERTICAL TUBES

Example sketches of some of the typical two-phase flow patterns (mist flow is not shown) occurring in a vertical tube are shown in Figure 1.8. The first five videos below show the transition from a bubbly flow to a slug flow via bubble clustering.

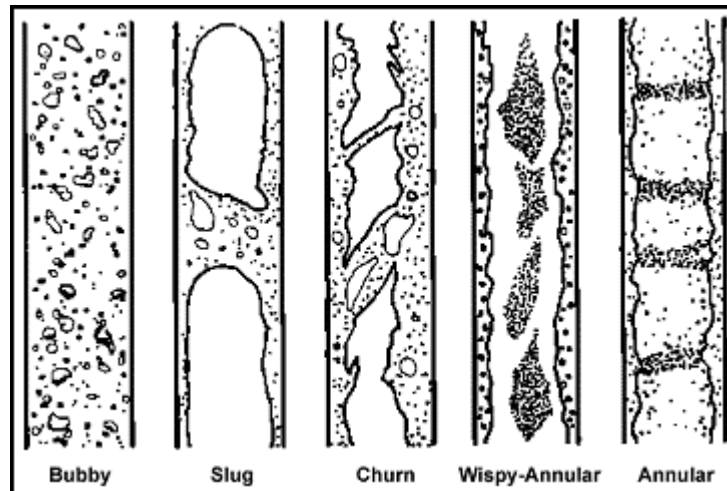


Figure 1.8. Illustration of two-phase flow patterns occurring in vertical evaporator tube.

List of videos: (click on the one you wish to see)

Video 1.4.1: *Dispersed bubble flow of air-water at void fraction of 5.1%.* The video shows a bubbly flow inside a vertical glass tube of 30 mm (1.181 in.) internal diameter. The liquid is water and the gas is air at ambient temperature. The flow is at a gas phase superficial velocity of 0.021 m/s and a liquid superficial velocity of 0.21 m/s. The flow depicts dispersed bubbles that have not yet begun to form into clusters. The video is at actual speed. The void fraction was measured using a microresistivity probe at the centerline of the channel. The videos were provided by the Laboratory for Fluid Dynamics and Thermodynamics (LFDT), Faculty of Mechanical Engineering, University of Ljubljana, Slovenia under the direction of Prof. Iztok Zun and were presented at the following international meeting: Zun and Polutnik (2001).

Video 1.4.2: *Bubbly flow of air-water at void fraction of 10.3% at start of clustering.* The video shows a bubbly flow inside a vertical glass tube of 30 mm (1.181 in.) internal diameter. The liquid is water and the gas is air at ambient temperature. The flow is at a gas phase superficial velocity of 0.029 m/s and a liquid

superficial velocity remains the same at 0.21 m/s. The flow depicts dispersed bubbles that have begun to form into clusters. The video is at actual speed. The void fraction was measured using a microresistivity probe at the centerline of the channel. The videos were provided by the Laboratory for Fluid Dynamics and Thermodynamics (LFDT), Faculty of Mechanical Engineering, University of Ljubljana, Slovenia under the direction of Prof. Iztok Zun and were presented at the following international meeting: Zun and Polutnik (2001).

Video 1.4.3: *Bubbly flow of air-water at void fraction of 13.9% with bubble clusters.* The video shows a bubbly flow with evident bubble clusters inside a vertical glass tube of 30 mm (1.181 in.) internal diameter. The liquid is water and the gas is air at ambient temperature. The flow is at a gas phase superficial velocity of 0.034 m/s and a liquid superficial velocity remains the same at 0.21 m/s. The flow depicts dispersed bubbles that have migrated together to form bubble clusters. The video is at actual speed. The void fraction was measured using a microresistivity probe at the centerline of the channel. The videos were provided by the Laboratory for Fluid Dynamics and Thermodynamics (LFDT), Faculty of Mechanical Engineering, University of Ljubljana, Slovenia under the direction of Prof. Iztok Zun and were presented at the following international meeting: Zun and Polutnik (2001).

Video 1.4.4: *Bubbly flow of air-water at void fraction of 15.4% with first slugs.* The video shows a bubbly flow with the first formation of slugs inside a vertical glass tube of 30 mm (1.181 in.) internal diameter. The liquid is water and the gas is air at ambient temperature. The flow is at a gas phase superficial velocity of 0.045 m/s and a liquid superficial velocity remains the same at 0.21 m/s. The flow depicts the point of transition of bubble clusters into vapor slugs with a high density of bubbles in the wake. The video is at actual speed. The void fraction was measured using a microresistivity probe at the centerline of the channel. The videos were provided by the Laboratory for Fluid Dynamics and Thermodynamics (LFDT), Faculty of Mechanical Engineering, University of Ljubljana, Slovenia under the direction of Prof. Iztok Zun and were presented at the following international meeting: Zun and Polutnik (2001).

Video 1.4.5: *Slug flow of air-water at void fraction of 17.0% with remaining bubbles.* The video shows a slug flow with numerous dispersed bubbles in the liquid phase inside a vertical glass tube of 30 mm (1.181 in.) internal diameter. The liquid is water and the gas is air at ambient temperature. The flow is at a gas phase superficial velocity of 0.058 m/s and a liquid superficial velocity remains the same at 0.21 m/s. The flow depicts well-established vapor slugs at these conditions. The video is at actual speed. The void fraction was measured using a microresistivity probe at the centerline of the channel. The videos were provided by the Laboratory for Fluid Dynamics and Thermodynamics (LFDT), Faculty of Mechanical Engineering, University of Ljubljana, Slovenia under the direction of Prof. Iztok Zun and were presented at the following international meeting: Zun and Polutnik (2001).

A study on the coalescence of two consecutive Taylor bubbles in a vertical tube has been investigated at the University of Tel Aviv by Profs. Shemer and Barnea. The videos were done for up flow of air and water in a very long vertical tube with an internal diameter of 25.0 mm (0.984 in.). The videos were taken at the University of Tel Aviv by C.A. Talvy under their direction. For a description of the test facility and their results, refer to: Talvy, Shemer and Barnea (2000) and Shemer, Gulitski and Barnea (2007).

Video 1.4.6: *Coalescence of two Taylor bubbles in a vertical tube.* The video shows a side view taken of a slug flow in a vertical tube (the tube itself is not visible in the video). The tests were done to study the influence of the separation distance between two consecutive bubbles upon the behavior of the trailing bubble. The higher speed of the trailing bubble and its collision with the upstream bubble is shown together with the deformation of the nose of the trailing bubble before the collision, all caused by the recirculating flow in the liquid slug between the bubbles (liquid currents are not visible in the video but can be inferred from the movement of small bubbles in the liquid slug).

Video 1.4.7: *Coalescence of Taylor bubbles in a vertical tube.* The video shows the side view of another slug flow in a vertical tube (the tube itself is not visible in the video). The trailing bubble collides with the upstream bubble but first the nose of the trailing bubble is severely disturbed before coalescence takes place. Also, the rear of the last bubble becomes highly unstable as this bubble accelerates to collide with the upstream bubble and is seen to break up into numerous small bubbles.

Numerous two-phase flow visualization studies in vertical tubes have been undertaken at the UKAEA Harwell Laboratory under the direction of Prof. G. Hewitt of Imperial College London. A selection of videos provided by Prof. Hewitt is shown below.

Video 1.4.8: *Axial view of annular flow in a vertical tube.* The video shows an axial view taken of annular flow in a vertical tube. The tests were done with up flow of water and air with the camera mounted at the top of the test section looking down the tube with laser light provided from the bottom of the test section for illumination. A large liquid entrainment in the central vapor core is clearly visible. The video was taken at UKAEA Harwell Laboratory by Dr. P. Whalley and Mr. Terry under direction of Prof. G. Hewitt. For a description of the test facility, refer to: Hewitt, Whalley and Terry (1979).

Video 1.4.9: *Side view of slug flow in a vertical tube with photochromatic dye tracing.* The video shows a side view taken of slug flow in a vertical tube with a photochromatic dye trace entering through the wall of the tube to indicate the direction of the local liquid flow. The direction of the flow is clearly visible, especially the flow reversal to down flow of the liquid film between the Taylor bubble and the wall. Also, the mixing in the liquid slug is clearly visible. The video was taken at UKAEA Harwell Laboratory under the direction of Prof. G. Hewitt. For a description of the test facility, refer to Walklate and Martin (1983).

Video 1.4.10: *Side view of churn flow in a vertical tube with photochromatic dye tracing.* The video shows a side view taken of churn flow in a vertical tube with a photochromatic dye trace entering through the wall of the tube to indicate the direction of the local liquid flow. The continuous gas flow through the core is clearly visible with waves carrying liquid upwards and falling liquid films between the waves. The video was taken at UKAEA Harwell Laboratory under the direction of Prof. G. Hewitt. For a description of the test facility, refer to Hewitt, Martin and Wilkes (1985).

1.5 ADIABATIC FALLING FILMS ON HORIZONTAL TUBE ARRAYS

Liquid films falling on horizontal tubes aligned as a vertical array (horizontal tubes one above the other) fall from tube to tube in distinct flow modes under the influence of gravity. As shown in Figure 1.9, the three principal intertube falling film flow modes are droplet, column and sheet, joined together by two transition regimes in which both droplets and columns coexist or columns and short sheets coexist. The videos illustrate these flows.

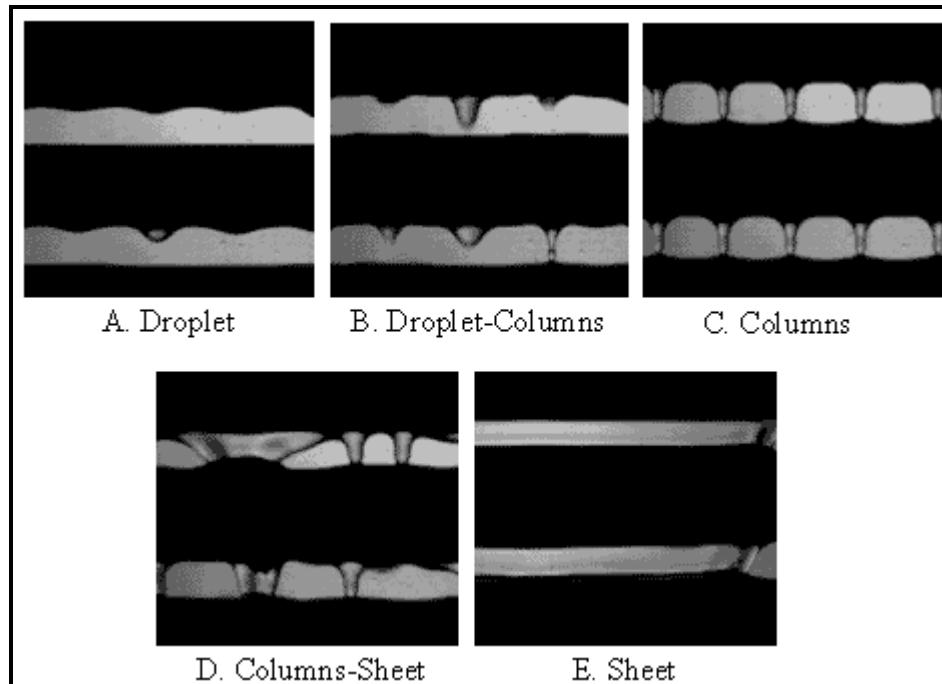


Figure 1.9. Diagram illustrating three principal intertube falling film flow modes on an array of horizontal tubes one below another (A, C and E) and the two transition regimes (B and D).

List of videos: (click on the one you wish to see)

Video 1.5.1: Droplet flow mode. The video shows the droplet flow mode from the bottom of the upper tube to the top of the lower tube. The tubes are plain with diameters of 19.05 mm (0.75 in.). The liquid is ethylene glycol falling in ambient air. The flow is near the transition to column flow mode as evidenced by the elongation of some of the liquid droplets into columns nearly reaching the lower tube. The video was obtained by J.F. Roques and V. Dupont in the Laboratory of Heat and Mass Transfer (LTCM) under the direction of Prof. J.R. Thome at the Swiss Federal Institute of Technology Lausanne (EPFL). The experimental test setup and work is described in: Roques, Dupont and Thome (2002).

Video 1.5.2: Transition from droplet to column flow mode. The video shows the transition in the flow regime from droplet flow mode to the column flow mode. The tubes are plain with diameters of 19.05 mm (0.75 in.). The liquid is ethylene glycol falling in ambient air. Both droplets and columns coexist along the tube, indicating the transition regime. The video was obtained by J.F. Roques and V. Dupont in the Laboratory of Heat and Mass Transfer (LTCM) under the direction of Prof. J.R. Thome at the Swiss Federal Institute of Technology Lausanne (EPFL). The experimental test setup and work is described in: Roques, Dupont and Thome (2002).

Video 1.5.3: Inline column flow mode. The video shows the inline column flow regime from the bottom of the upper tube onto the top of the lower tube. The tubes are plain with diameters of 19.05 mm (0.75 in.). The liquid is ethylene glycol falling in ambient air. The columns are very stable (difficult to see any movement) and nearly equally spaced. The video was obtained by J.F. Roques and V. Dupont in the Laboratory of Heat and Mass Transfer (LTCM) under the direction of Prof. J.R. Thome at the Swiss Federal Institute of Technology Lausanne (EPFL). The experimental test setup and work is described in: Roques, Dupont and Thome (2002).

Video 1.5.4: Staggered column flow mode. The video shows the staggered column flow regime from the bottom of the upper tube onto the top of the lower tube. The tubes are plain with diameters of 19.05 mm (0.75 in.). The liquid is ethylene glycol falling in ambient air. The columns are quite stable and nearly equally spaced and equally staggered. The staggered regime is achieved by increasing the film flow rate, which creates a crest of liquid at the top of the tube between impinging liquid jets. The thick liquid layer at a crest then flows around the tube to form the staggered column on the bottom. The video was obtained by J.F. Roques and V. Dupont in the Laboratory of Heat and Mass Transfer (LTCM) under the direction of Prof. J.R. Thome at the Swiss Federal Institute of Technology Lausanne (EPFL). The experimental test setup and work is described in: Roques, Dupont and Thome (2002).

Video 1.5.5: Transition from column to sheet flow mode. The video shows the transition from the staggered column flow regime to the sheet flow regime at intervals along the tube. The tubes are plain with diameters of 19.05 mm (0.75 in.). The liquid is ethylene glycol falling in ambient air. The short width of the sheets renders them unstable and surface tension pulls them into a wedge shape. Columns and small sheets tend to coalesce. The video was obtained by J.F. Roques and V. Dupont in the Laboratory of Heat and Mass Transfer (LTCM) under the direction of Prof. J.R. Thome at the Swiss Federal Institute of Technology Lausanne (EPFL). The experimental test setup and work is described in: Roques, Dupont and Thome (2002).

Video 1.5.6: Sheet flow mode. The video shows the sheet flow regime from the bottom of the upper tube to the top of the lower tube, i.e. the classic flow regime assumed for falling film condensation on tube rows by Nusselt (1916). The tubes are plain with diameters of 19.05 mm (0.75 in.). The liquid is ethylene glycol falling in ambient air. The surface tension forces on the ends of the sheet tend to pull them in. The video was obtained by J.F. Roques and V. Dupont in the Laboratory of Heat and Mass Transfer (LTCM) under the direction of Prof. J.R. Thome at the Swiss Federal Institute of Technology Lausanne (EPFL). The experimental test setup and work is described in: Roques, Dupont and Thome (2002).

Video 1.5.7: Slow motion of transition from droplet to column mode. The video shows a slow motion of a video out the transition of droplets to columns. The tubes are plain with diameters of 19.05 mm (0.75 in.). The liquid is water falling in ambient air. The original digital video was taken at 1000 images per second and has been slowed down for viewing. The video was obtained by J.F. Roques and V. Dupont in the Laboratory of Heat and Mass Transfer (LTCM) under the direction of Prof. J.R. Thome at the Swiss Federal Institute of Technology Lausanne (EPFL). The experimental test setup and work is described in: Roques, Dupont and Thome (2002).

Video 1.5.8: Falling film of R-134a on plain tube at low flow rate. The video shows flow of liquid R-134a film on plain tubes of 19.05 mm (0.75 in.) with intertube spacing of 9.5 mm (0.374 in.). The R-134a is at a saturation temperature of 20°C (68°F) with a flow rate per unit length of tube equal to 0.07 kg/m s (0.047 lb/ft s). The flow mode is near the transition from droplet to column mode (predominately droplet flow is observed) but the droplet flow is rather unstable. The video was obtained by D. Gstöhl and J.F. Roques in the Laboratory of Heat and Mass Transfer (LTCM) under the direction of Prof. J.R. Thome at the Swiss Federal Institute of Technology Lausanne (EPFL).

Video 1.5.9: Falling film of R-134a on plain tube at medium flow rate. The video shows flow of liquid R-134a film on plain tubes of 19.05 mm (0.75 in.) with intertube spacing of 9.5 mm (0.374 in.). The R-134a is at a saturation temperature of 20°C (68°F) with a flow rate per unit length of tube equal to 0.11 kg/m s (0.074 lb/ft s). The flow mode is column but they are rather unstable and cause some liquid to sling laterally off the bottom of the tube, typically observed in numerous other occasions. The video was obtained by D. Gstöhl and J.F. Roques in the Laboratory of Heat and Mass Transfer (LTCM) under the direction of Prof. J.R. Thome at the Swiss Federal Institute of Technology Lausanne (EPFL).

Video 1.5.10: *Falling film of R-134a on plain tube at high flow rate.* The video shows flow of liquid R-134a film on plain tubes of 19.05 mm (0.75 in.) with intertube spacing of 9.5 mm (0.374 in.). The R-134a is at a saturation temperature of 20°C (68°F) with a flow rate per unit length of tube equal to 0.36 kg/m s (0.241 lb/ft s). The flow mode is near the transition from column to sheet but the liquid columns are unstable and cause some liquid to sling laterally off the bottom of the tube, typically observed in numerous other occasions. The video was obtained by D. Gstöhl and J.F. Roques in the Laboratory of Heat and Mass Transfer (LTCM) under the direction of Prof. J.R. Thome at the Swiss Federal Institute of Technology Lausanne (EPFL).

1.6 FALLING FILM CONDENSATION ON HORIZONTAL TUBES

Condensation on horizontal tube bundles is a common process with the condensate from above tubes inundating the lower tubes. Hence, the condensate flowing from an upper tube to a lower tube characterizes the two-phase flow regime, called the intertube flow mode here.

List of videos: (click on the one you wish to see)

Video 1.6.1: *R-134a condensing on tube array in droplet mode flow.* The video shows R-134a condensing at 30°C (86°F) on the second tube of an array of tubes. The tubes are plain with diameters of 19.05 mm (0.75 in.) and the intertube spacing is 6.4 mm (0.25 in.). The heat flux on the second tube is 6400 W/m² (2030 Btu/h ft²). The flow is in the droplet mode. Elongation of the droplets during their departure is clearly visible and the spreading of the condensate upon impact on the lower tube. The video was taken by D. Gstöhl in the Laboratory of Heat and Mass Transfer (LTCM) under the direction of Prof. J.R. Thome at the Swiss Federal Institute of Technology Lausanne (EPFL). The experimental test setup is described in Gstöhl and Thome (2006c).

Video 1.6.2: *R-134a condensing on tube array in droplet mode near transition to column flow.* The video shows R-134a condensing at 30°C (86°F) on the sixth tube of an array of tubes. The tubes are plain with diameters of 19.05 mm (0.75 in.) and the intertube spacing is 6.4 mm (0.25 in.). The heat flux on the sixth tube is 8100 W/m² (2670 Btu/h ft²). The flow is in the droplet mode near the transition to column flow. The elongating droplets are unstable and perhaps this prevents the formation of stable columns at this condition. The video was taken by D. Gstöhl in the Laboratory of Heat and Mass Transfer (LTCM) under the direction of Prof. J.R. Thome at the Swiss Federal Institute of Technology Lausanne (EPFL). The experimental test setup is described in Gstöhl and Thome (2006c).

Video 1.6.3: *R-134a condensing on tube array in column mode.* The video shows R-134a condensing at 30°C (86°F) on the sixth tube of an array of tubes. The tubes are plain with diameters of 19.05 mm (0.75 in.) and the intertube spacing is 6.4 mm (0.25 in.). The heat flux on the sixth tube is 20000 W/m² (6340 Btu/h ft²). The flow is in the column mode and the columns are unstable. The video was taken by D. Gstöhl in the Laboratory of Heat and Mass Transfer (LTCM) under the direction of Prof. J.R. Thome at the Swiss Federal Institute of Technology Lausanne (EPFL). The experimental test setup is described in Gstöhl and Thome (2006c).

Video 1.6.4: *R-134a condensing on 6-tube array at low heat flux in droplet mode.* The video shows R-134a condensing at 30°C (86°F) on a six-tube array. The tubes are plain with diameters of 19.05 mm (0.75 in.) and the intertube spacing is 6.4 mm (0.25 in.). The heat flux on the top tube is 9500 W/m² (3010 Btu/h ft²) and on the bottom tube is 6700 W/m² (2120 Btu/h ft²). The flow is in the droplet mode from all tubes. The video was taken by D. Gstöhl in the Laboratory of Heat and Mass Transfer (LTCM) under the direction of Prof. J.R. Thome at the Swiss Federal Institute of Technology Lausanne (EPFL). The experimental test setup is described in Gstöhl and Thome (2006c).

Video 1.6.5: *R-134a condensing on 6-tube array at medium heat flux going from droplet to column mode.* The video shows R-134a condensing at 30°C (86°F) on a six-tube array. The tubes are plain with diameters of 19.05 mm (0.75 in.) and the intertube spacing is 6.4 mm (0.25 in.). The heat flux on the top tube is 26000 W/m² (8240 Btu/h ft²) and on the bottom tube is 20000 W/m² (6340 Btu/h ft²). The flow is in the droplet mode at the top and progresses to column mode at the bottom. The video was taken by D. Gstöhl in the Laboratory of Heat and Mass Transfer (LTCM) under the direction of Prof. J.R. Thome at the Swiss Federal Institute of Technology Lausanne (EPFL). The experimental test setup is described in Gstöhl and Thome (2006c).

1.7 FALLING FILM EVAPORATION ON HORIZONTAL TUBES

Falling film evaporation on horizontal tube bundles is becoming an important process in refrigeration systems, in which liquid is overfeed onto the top tube of an array of horizontal tubes and evaporates as the liquid falls under the influence of gravity. The liquid flow rate thus decreases progressively from tube to tube as it evaporates. The flow of the liquid film from tube to tube is characterized by the two-phase flow regime, called the intertube flow mode here. As can be seen in some of the videos below, heat transfer is not only by conduction or convection across the film but also by nucleate boiling on the tube wall within the film. This tends to create a mist of minute droplets of liquid and in some videos the “fog” created is visible.

List of videos: (click on the one you wish to see)

Video 1.7.1: *R-134a evaporating on array of plain tubes with partial dryout.* The video shows R-134a evaporating at 5°C (41°F) on an array of seven tubes. The tubes are plain with diameters of 19.05 mm (0.75 in.) and the intertube spacing is 6.4 mm (0.25 in.). The heat flux on the top tube is 55000 W/m² (17440 Btu/h ft²) and 30000 W/m² (9510 Btu/h ft²) on the bottom tube. The flow is mostly column mode with large instabilities. The video was taken by J.F. Roques in the Laboratory of Heat and Mass Transfer (LTCM) under the direction of Prof. J.R. Thome at the Swiss Federal Institute of Technology Lausanne (EPFL). For a description of the falling film heat transfer test facility, refer to: Roques (2004).

Video 1.7.2: *R-134a evaporating on array of plain tubes with nearly complete dryout.* The video shows R-134a evaporating at 5°C (41°F) on an array of seven tubes. The tubes are plain with diameters of 19.05 mm (0.75 in.) and the intertube spacing is 6.4 mm (0.25 in.). The heat flux on the top tube is 96000 W/m² (30440 Btu/h ft²) and 3000 W/m² (950 Btu/h ft²) on the bottom tube. The flow is mostly column mode with large instabilities and then droplet flow at the bottom. The film is nearly completely dried out on the lowest tube. The video was taken by J.F. Roques in the Laboratory of Heat and Mass Transfer (LTCM) under the direction of Prof. J.R. Thome at the Swiss Federal Institute of Technology Lausanne (EPFL). For a description of the falling film heat transfer test facility, refer to: Roques (2004).

Video 1.7.3: *Close up of nucleate boiling on top of tube with falling liquid film (droplet mode).* The video shows R-134a evaporating at 5°C (41°F) on an array of tubes. The tubes are plain with diameters of 19.05 mm (0.75 in.) and the intertube spacing is 6.4 mm (0.25 in.). The film flow is in droplet mode and nucleate boiling with bubbles erupting in the spreading film on the lower tube is clearly visible. The video was taken by J.F. Roques in the Laboratory of Heat and Mass Transfer (LTCM) under the direction of Prof. J.R. Thome at the Swiss Federal Institute of Technology Lausanne (EPFL). For a description of the falling film heat transfer test facility, refer to: Roques (2004).

Video 1.7.4: *Nucleate boiling and dryout on top of tube in droplet mode.* The video shows R-134a evaporating at 5°C (41°F) on an array of tubes. The tubes are plain with diameters of 19.05 mm (0.75 in.)

and the intertube spacing is 6.4 mm (0.25 in.). The film flow is in droplet mode and nucleate boiling occurs in the liquid film on the tube. Note the bubbles inside the droplets leaving the lower tube. Small liquid droplets created by the nucleate boiling process are also notable. The video was taken by J.F. Roques in the Laboratory of Heat and Mass Transfer (LTCM) under the direction of Prof. J.R. Thome at the Swiss Federal Institute of Technology Lausanne (EPFL). For a description of the falling film heat transfer test facility, refer to: Roques (2004).

Video 1.7.5: *Film condensation on upper tube with nucleate boiling in film on lower tube.* The video shows R-134a condensing on the upper tube (with cooling water inside tube) and evaporating on lower tube (hot water inside tube). The tubes are plain with diameters of 19.05 mm (0.75 in.) and the intertube spacing is 6.4 mm (0.25 in.). The film flow is in droplet mode and nucleate boiling is quite evident in the liquid film on the tube. The video was taken by J.F. Roques in the Laboratory of Heat and Mass Transfer (LTCM) under the direction of Prof. J.R. Thome at the Swiss Federal Institute of Technology Lausanne (EPFL). For a description of the falling film heat transfer test facility, refer to: Roques (2004).

Video 1.7.6: *Close up of nucleate boiling in film on lower tube (reverse shading).* The video shows R-134a evaporating on lower tube with nucleate boiling in the liquid film, inverting the black and white images. The tubes are plain with diameters of 19.05 mm (0.75 in.) and the intertube spacing is 6.4 mm (0.25 in.). The video was taken by J.F. Roques in the Laboratory of Heat and Mass Transfer (LTCM) under the direction of Prof. J.R. Thome at the Swiss Federal Institute of Technology Lausanne (EPFL). For a description of the falling film heat transfer test facility, refer to: Roques (2004).

1.8 POOL BOILING

Pool boiling is a fundamental process in two-phase heat transfer. Pool boiling is a two-phase natural convection process created by the buoyancy of the vapor bubbles, creating very dynamic and complex phenomena.

List of videos: (click on the one you wish to see)

The videos shown below document the pool boiling process on a flat, circular heated plate over all regimes of the pool boiling curve obtained in the same tests. The videos were taken for boiling on a heated copper test surface facing upwards with a 35 mm (1.4 in.) diameter situated at the bottom of a large boiling vessel. At the top of the videos, a 3D-movable micro-thermocouple probe and a micro-optical probe, respectively, are visible. The tests were carried out with saturated isopropanol at a pressure of 0.106 MPa (15.4 psia) and a saturation temperature of 83.3°C (182°F). All experiments are carried out under steady-state conditions. The surface temperature of the temperature-controlled test heater was fixed at five different temperatures as indicated on their pool boiling curve obtained for this test surface in Figure 1.10. Their five videos show all the important boiling regimes: low heat flux nucleate boiling (1st Video), developed nucleate boiling at higher heat flux (2nd Video), departure from nucleate boiling DNB (3rd Video), transition boiling (4th Video) and film boiling (5th Video). The videos were taken by Prof. H. Auracher, Prof. F. Ziegler and O. Koeppen at the Institut für Energietechnik, Technische Universität Berlin. More details about the test facility and visualizations are available in Buchholz (2005) and Buchholz et al. (2004).

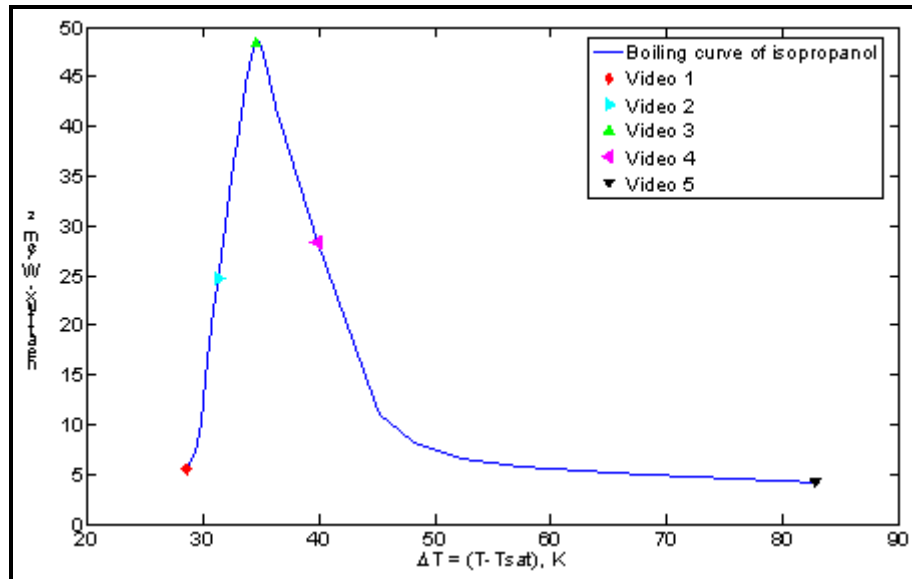


Figure 1.10. Pool boiling curve of Buchholz et al. (2004) for isopropanol showing the test conditions of their five videos.

[Video 1.8.1](#): Low heat flux nucleate pool boiling on a horizontal surface.

[Video 1.8.2](#): Developed nucleate pool boiling on a horizontal surface.

[Video 1.8.3](#): Departure from nucleate boiling (DNB) on a horizontal surface.

[Video 1.8.4](#): Transition boiling on a horizontal surface.

[Video 1.8.5](#): Film boiling on a horizontal surface.

1.9 MICROCHANNEL TWO-PHASE FLOW PHENOMENA

Two-phase flow in microchannels is a process of growing industrial importance in compact heat exchangers and electronic cooling modules. The criterion to define the threshold from macro-scale to micro-scale two-phase flow and heat transfer is still not resolved but typically at normal operating pressures is taken to be at about 1-2 mm for the internal diameter of the channel. New flow pattern maps have been proposed and others are under development to describe and identify these flow regimes. Here some representative videos are shown.

List of videos: (click on the one you wish to see)

A large number of videos for two-phase flows in glass microchannels located at the exit of a microchannel evaporator of the same internal diameter have been taken by R. Revellin during his Ph.D. thesis in the Laboratory of Heat and Mass Transfer (LTCH) under the direction of Prof. J.R. Thome at the Swiss Federal Institute of Technology Lausanne (EPFL). Three sizes of microchannels were tested: 2.0, 0.8 and 0.5 mm internal diameters (0.0787, 0.0315 and 0.0197 in.) and also two refrigerants: R-134a and R-245fa. The experimental setup and observations are described in Revellin (2005), Revellin et al. (2006) and Revellin and Thome (2007). For the elongated bubble regimes in the two smaller microchannels, the bubble velocities and bubble lengths were determined by image processing of the videos shown here (plus

others), where the results are available in Agostini, Revellin and Thome (2007). A large selection of these videos is shown below. Only one video for the largest channel is shown. For the smaller two test sections, the test conditions are cited in each individual video itself.

2.0 mm channel with R-134a: One video at one mass velocity is shown.

Video 1.9.1: *Elongated bubble (slug) flow in a 2.0 mm microchannel tube.* The video shows R-134a in a 2.0 mm (0.079 in.) internal diameter glass tube located at the exit of a microchannel evaporation test section at room temperature. The length to diameter ratio of the elongated bubbles is larger than in macroscale channels. Note also the effect of buoyancy on the bubble that produces a much thinner liquid film at the top of the elongated bubble than at the bottom.

0.5 mm channel with R-134a at 360 kg/m²s: Seven videos over a range of vapor qualities at this nominal mass velocity are shown below (actual mass velocity is cited in the individual video).

Video 1.9.2: 2.9% vapor quality

Video 1.9.3: 3.7% vapor quality

Video 1.9.4: 5.0% vapor quality

Video 1.9.5: 6.8% vapor quality

Video 1.9.6: 9.0% vapor quality

Video 1.9.7: 13.7% vapor quality

Video 1.9.8: 19.4% vapor quality

0.5 mm channel with R-134a at 520 kg/m²s: Nine videos over a range of vapor qualities at this nominal mass velocity are shown below (actual mass velocity is cited in the individual video).

Video 1.9.9: 2.6% vapor quality

Video 1.9.10: 3.2% vapor quality

Video 1.9.11: 5.7% vapor quality

Video 1.9.12: 10.4% vapor quality

Video 1.9.13: 16.5% vapor quality

Video 1.9.14: 24.0% vapor quality

Video 1.9.15: 39.0% vapor quality

Video 1.9.16: 60.9% vapor quality

Video 1.9.17: 80.3% vapor quality

0.5 mm channel with R-134a at 1500 kg/m²s: Five videos over a range of vapor qualities at this nominal mass velocity are shown below (actual mass velocity is cited in the individual video).

Video 1.9.18: 1.3% vapor quality

Video 1.9.19: 1.9% vapor quality

Video 1.9.20: 2.6% vapor quality

Video 1.9.21: 3.9% vapor quality

Video 1.9.22: 5.3% vapor quality

0.5 mm channel with R-245fa at 520 kg/m²s: Ten videos over a range of vapor qualities at this nominal mass velocity are shown below (actual mass velocity is cited in the individual video).

Video 1.9.23: 3.8% vapor quality

Video 1.9.24: 4.0% vapor quality

Video 1.9.25: 4.7% vapor quality

[Video 1.9.26](#): 6.0% vapor quality

[Video 1.9.27](#): 7.9% vapor quality

[Video 1.9.28](#): 9.7% vapor quality

[Video 1.9.29](#): 11.9% vapor quality

[Video 1.9.30](#): 14.9% vapor quality

[Video 1.9.31](#): 22.9% vapor quality

[Video 1.9.32](#): 40.4% vapor quality

0.5 mm channel with R-245fa at 1010 kg/m²s: Six videos over a range of vapor qualities at this nominal mass velocity are shown below (actual mass velocity is cited in the individual video).

[Video 1.9.33](#): 3.9% vapor quality

[Video 1.9.34](#): 4.2% vapor quality

[Video 1.9.35](#): 4.7% vapor quality

[Video 1.9.36](#): 6.1% vapor quality

[Video 1.9.37](#): 7.7% vapor quality

[Video 1.9.38](#): 13.4% vapor quality

0.5 mm channel with R-245fa at 1520 kg/m²s: Three videos over a range of vapor qualities at this nominal mass velocity are shown below (actual mass velocity is cited in the individual video).

[Video 1.9.39](#): 4.8% vapor quality

[Video 1.9.40](#): 5.4% vapor quality

[Video 1.9.41](#): 6.5% vapor quality

0.8 mm channel with R-134a at 200 kg/m²s: Eleven videos over a range of vapor qualities at this nominal mass velocity are shown below (actual mass velocity is cited in the individual video).

[Video 1.9.42](#): 2.9% vapor quality

[Video 1.9.43](#): 3.9% vapor quality

[Video 1.9.44](#): 5.7% vapor quality

[Video 1.9.45](#): 7.6% vapor quality

[Video 1.9.46](#): 11.7% vapor quality

[Video 1.9.47](#): 16.1% vapor quality

[Video 1.9.48](#): 22.2% vapor quality

[Video 1.9.49](#): 30.5% vapor quality

[Video 1.9.50](#): 40.7% vapor quality

[Video 1.9.51](#): 52.3% vapor quality

[Video 1.9.52](#): 65.2% vapor quality

0.8 mm channel with R-134a at 510 kg/m²s: Nine videos over a range of vapor qualities at this nominal mass velocity are shown below (actual mass velocity is cited in the individual video).

[Video 1.9.53](#): 2.9% vapor quality

[Video 1.9.54](#): 3.7% vapor quality

[Video 1.9.55](#): 5.2% vapor quality

[Video 1.9.56](#): 7.8% vapor quality

[Video 1.9.57](#): 9.6% vapor quality

[Video 1.9.58](#): 23.6% vapor quality

[Video 1.9.59](#): 29.3% vapor quality

[Video 1.9.60](#): 37.4% vapor quality

[Video 1.9.61](#): 72.5% vapor quality

0.8 mm channel with R-134a at 1010 kg/m²s: Nine videos over a range of vapor qualities at this nominal mass velocity are shown below (actual mass velocity is cited in the individual video).

[Video 1.9.62](#): 0.7% vapor quality

[Video 1.9.63](#): 1.1% vapor quality

[Video 1.9.64](#): 1.6% vapor quality

[Video 1.9.65](#): 2.4% vapor quality

[Video 1.9.66](#): 3.3% vapor quality

[Video 1.9.67](#): 5.1% vapor quality

[Video 1.9.68](#): 7.4% vapor quality

[Video 1.9.69](#): 13.3% vapor quality

[Video 1.9.70](#): 28.5% vapor quality

0.8 mm channel with R-134a at 1500 kg/m²s: Six videos over a range of vapor qualities at this nominal mass velocity are shown below (actual mass velocity is cited in the individual video).

[Video 1.9.71](#): 0.5% vapor quality

[Video 1.9.72](#): 0.7% vapor quality

[Video 1.9.73](#): 1.3% vapor quality

[Video 1.9.74](#): 2.0% vapor quality

[Video 1.9.75](#): 3.2% vapor quality

[Video 1.9.76](#): 4.2% vapor quality

A series of five videos of evaporating flows at high heat fluxes in triangular cross-sectional microchannels with a transparent top plate have been taken at the Technion University under the direction of Prof. G. Hetsroni in Israel. The test fluid is water. The parallel microchannels are made in a silicon plate and have a hydraulic diameter of 0.130 mm (0.005 in.). The experimental setup and observations are described in Hetsroni (2005) and Hetsroni et al. (2002, 2003).

[Video 1.9.77](#): *Overall view of the multi-microchannel test section.* The video shows several views of the test section used to obtain the high speed videos of the boiling process in the microchannels.

[Video 1.9.78](#): *View of boiling in a multi-microchannel test section.* The video shows a large view of the boiling process in the microchannels for a fluid velocity of 0.095 m/s (0.31 ft/s) at a heat flux of 124 kW/m² (39300 Btu/h ft²).

[Video 1.9.79](#): *Bubble burst in a channel of the multi-microchannel test section.* The video shows the burst of a large bubble during boiling in their microchannel test section with quasi-periodic dryout for a superficial liquid velocity of 0.075 m/s (0.246 ft/s) and a heat flux of 240 kW/m² (76100 Btu/h ft²).

[Video 1.9.80](#): *Dryout in several channels of the multi-microchannel test section.* The video shows the dryout process in neighboring channels during boiling in their microchannel test section (this one with a hydraulic diameter of 0.160 mm rather than 0.130 mm) with a superficial liquid velocity of 0.075 m/s (0.246 ft/s) and a heat flux of 140 kW/m² (44400 Btu/h ft²).

[Video 1.9.81](#): *Intermittent dryout with rewetting of a channel.* The video shows “explosive boiling” in a microchannel for a superficial liquid velocity of 0.095 m/s (0.31 ft/s) and a heat flux of 124 kW/m² (39300 Btu/h ft²). The field of view is 0.6 mm by 1.0 mm.

A series of videos of evaporating flows in horizontal, transparent glass microchannels have been taken at the Department of Mechanical Engineering, The University of Tokyo under the direction of Prof. N. Kasagi by Tzu-Hsiang Yen using R-123 as the test fluid. The two videos below were taken at a speed of 24,000 images per second and are shown in slow motion here. The videos show boiling nucleation at the channel wall, bubble growth, backflow and rewetting of the channel. The experimental setup and descriptions of their observations are presented in Yen et al. (2005) and Yen et al. (2006).

Video 1.9.82: *Flow pattern variation in a horizontal circular microchannel (1st Video)*. The video displays the variation in the flow patterns of convective boiling inside a horizontal, circular microchannel of 0.21 mm (0.0083 in.) diameter at a mass flux of 400 kg/m²s (294000 lb/h ft²), a heat flux of 37.53 kW/m² (11900 Btu/h ft²) and vapor quality of 0.074. The test fluid is R-123 and the tests were at a saturation temperature of 27°C (81°F) at 1.01 bar. Compared to the square channel below, fewer nucleation bubbles are generated and the period of flow pattern variation is shorter, while the variation of flow patterns is more complex. The video was taken by Tzu-Hsiang Yen in collaboration with Profs. N. Kasagi and M. Shoji. For a description of the test facility and detailed discussion of the phenomena, refer to: Yen et al. (2006).

Video 1.9.83: *Flow pattern variation in a horizontal square microchannel (2nd Video)*. The video displays the variation in the flow patterns of convective boiling inside a horizontal, square cross-sectional microchannel of 0.214 mm (0.0084 in.) hydraulic diameter at a mass flux of 400 kg/m²s (294000 lb/h ft²), a heat flux of 39.25 kW/m² (12400 Btu/h ft²) and a vapor quality of 0.069. The fluid is R-123 and the experimental conditions for this square channel are very similar to those of the circular channel above. Bubbles grow in both the downstream and upstream directions of the tube due to the very limited space in the microchannel, leading to a quasi-periodic flow pattern variation from bubbly to annular flow patterns at the same observation point. The video was taken by Tzu-Hsiang Yen in collaboration with Prof. N. Kasagi at The University of Tokyo and Prof. M. Shoji at the Energy Technology Institute, National Institute of Advanced Industrial Science and Technology (AIST). For a description of the test facility and detailed discussion of the phenomena, refer to: Yen et al. (2006).

A series of videos of capillary condensing flows in a horizontal, transparent glass microchannel have been taken at the Laboratoire d'Energétique at the Université Paul Sabatier in Toulouse, France by B. Médéric, P. Lavieille and M. Miscevic. The test fluid is n-pentane at atmospheric pressure. Using a syringe pump, the mass velocities in the videos ranged from 9 to 14 kg/m²s (6600 to 10300 lb/h ft²). The glass channel has a diameter of 0.56 mm (0.022 in.). The vapor enters slightly superheated and partially condenses at a saturation temperature of 36°C (97°F). The five videos below were taken at a speed of 25 images per second and show elongated vapor bubbles with condensation at their interface with subsequent break off and flow downstream. The experimental setup, descriptions of their observations and void fraction measurements using their image processing technique are described in Médéric, Lavieille and Miscevic (2005).

Video 1.9.84: *Capillary condensation in a glass microchannel (1st Video)*. This video shows an oscillating elongated bubble at a mass velocity of 9 kg/m²s (6600 lb/h ft²).

Video 1.9.85: *Capillary condensation in a glass microchannel (2nd Video)*. This video shows an oscillating elongated bubble with rapid detachment of bubbles at a mass velocity of 11 kg/m²s (8100 lb/h ft²).

Video 1.9.86: *Capillary condensation in a glass microchannel (3rd Video)*. This video shows an oscillating elongated bubble at a mass velocity of 14 kg/m²s (10300 lb/h ft²).

Video 1.9.87: *Capillary condensation in a glass microchannel (4th Video)*. This video shows an oscillating elongated bubble splitting into small bubbles at a mass velocity of $14 \text{ kg/m}^2\text{s}$ (10300 lb/h ft^2).

Video 1.9.88: *Capillary condensation in a glass microchannel (5th Video)*. This video shows a flow of condensing bubbles at a mass velocity of $14 \text{ kg/m}^2\text{s}$ (10300 lb/h ft^2).

Videos of evaporating flows in a square matrix of silicon microchannels with a glass cover plate have been taken at the Heat Transfer Laboratory at the University of Houston by T. Cognata under the direction of Prof. K. Hollingsworth and Prof. L. Witte. The test fluid is R-11. The micro-heat exchanger is made from a DNA micro-array adapted for use as an evaporator. The channels are 0.050 mm (0.002 in.) wide separated by 0.150 mm (0.006 in.) silicon posts in a 45° alignment to the direction of flow. Using a syringe pump, the liquid enters at the right and partially evaporates as it flows to the left. The four videos were taken at a speed of 5000 images per second and show nucleation, short and elongated vapor bubbles and annular flow. The experimental setup, descriptions of their observations and heat transfer measurements are described in Cognata, Hollingsworth and Witte (2006).

Video 1.9.89: *Two-phase flow in a microscale heat exchanger (1st Video)*. This video shows evaporation at a heat flux of 50 kW/m^2 (15850 Btu/h ft^2) at a mass velocity of $141 \text{ kg/m}^2\text{s}$ (104000 lb/h ft^2) at the central zone of the test section.

Video 1.9.90: *Two-phase flow in a microscale heat exchanger (2nd Video)*. This video shows evaporation at a heat flux of 50 kW/m^2 (15850 Btu/h ft^2) at a mass velocity of $141 \text{ kg/m}^2\text{s}$ (104000 lb/h ft^2) at the inlet zone of the test section.

Video 1.9.91: *Magnified view of bubble flow in a microscale heat exchanger (3rd Video)*. This video shows the evaporation process at a heat flux of 50 kW/m^2 (15850 Btu/h ft^2) at a mass velocity of $141 \text{ kg/m}^2\text{s}$ (104000 lb/h ft^2) at the exit zone of the test section.

Video 1.9.92: *Magnified view of bubble flow in a microscale heat exchanger (3rd Video)*. This video shows a highly magnified view of the evaporation process for elongated bubbles at the intersection of several microchannels.

A video of evaporation at high heat flux was taken in a joint project between Profs. Xu, Gan, Zhang and Li of the Guagnzhou Institute of Energy Conversion of the Chinese Academy of Science, the Department of Thermal and Energy Engineering at the University of Science and Technology of China in Hefei and the Institute of Microelectronics at Peking University, Beijing, respectively. The test fluid was acetone. The ten parallel microchannels were made in a silicon plate with a hydraulic diameter of 0.1554 mm (0.006 in.). They are triangular in cross-section with a width of 0.300 mm (0.012 in.) at the top with the viewing plate and 0.212 mm deep (0.008 in.). The experimental setup, descriptions of their observations and analysis are presented in detail in Xu et al. (2005).

Video 1.9.93: *Nucleation and rapid dryout in a multi-microchannel element*. The video shows a slow motion view of the activation of multiple nucleation sites followed by very rapid vaporization at a heat flux of 142 kW/m^2 (45000 Btu/h ft^2) and a liquid Reynolds number of 65.2. When the channels become “black” this means that they have dried out. The process is cyclical and the video shows one cycle of the process.

1.10 SINGLE-PHASE FLOW PHENOMENA

List of videos: (click on the one you wish to see)

No videos currently available.

1.11 CRITICAL HEAT FLUX IN AN ANNULUS

Critical heat flux (CHF) is an important diabatic two-phase phenomenon in saturated and subcooled flow boiling. It designates the departure from wet wall cooling of the heated channel by the liquid at high heat flux and is associated with a rapid rise in the wall temperature that may result in burnout of the test section if the applied heating is not cut off in time. For a description of a mechanistic model of CHF in subcooled boiling, refer to Celata et al. (1999) while the empirical CHF correlation of Katto and Ohno (1984) for saturated and subcooled CHF is presented elsewhere in this book.

Celata, Cumo and Mariani (1999) and Celata et al. (2000) have taken digital videos of the CHF process occurring in an annulus. Their test section is described in Figure 1.11. Two of the four walls of the square flow channel are made of Plexiglas so that the laser light is able to pass through these two transparent plates and thus illuminates the surface of the heater on which the boiling phenomena occurs. The other two walls are stainless steel. The heated surface is a solid cylindrical rod placed at the center of the square duct. The inside dimension of the square duct is 7.2 mm (0.28 in.). The cylindrical heater is 2 mm (0.079 in.) in diameter and 100 mm (3.94 in.) in length. The heater, one for each run, is made of stainless steel 316L and is uniformly heated over its length by Joule effect up to 90 kW.

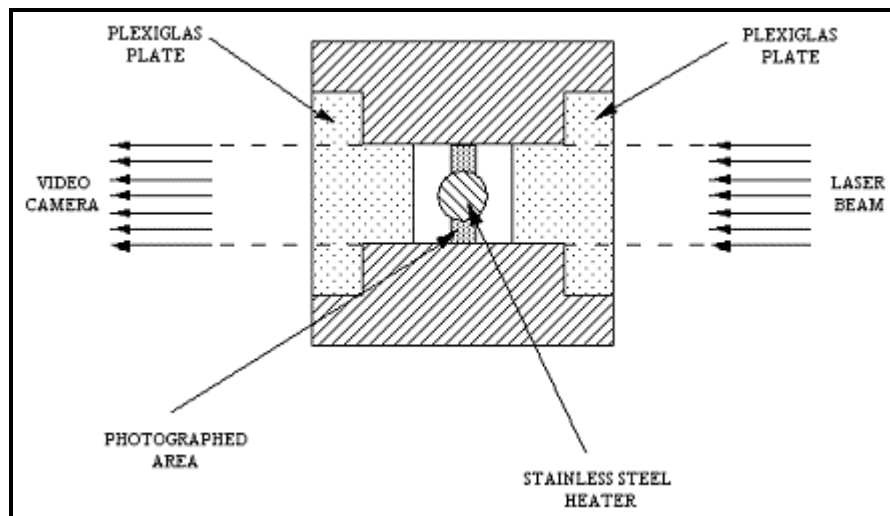


Figure 1.11. Schematic diagram of the CHF test section of Celata and coworkers.

Six videos from the above studies are shown below (one at normal speed and the second at slow motion for each of the three conditions). They were taken at ENEA Casaccia by A. Marianni and G. Zummo at the Institute of Thermal-Fluid Dynamics in Rome, Italy under the direction of Dr. G.P. Celata. The test fluid is demineralized water.

List of videos: (click on the one you wish to see)

[Video 1.11.1](#) and [video 1.11.2](#) (slow motion): *CHF in an Annulus (1st run)*. The videos display CHF occurring at the following test conditions: inlet temperature is 20°C (68°F), outlet temperature is 32°C (89.6°F), outlet pressure is 2 bar (29.0 psia), inlet subcooling is 100 K (180°F), mass velocity is 2160 kg/m²s (1590000 lb/hft²) and liquid velocity is 2.2 m/s (7.2 ft/s). The heat flux of CHF in this video was 3900 kW/m² (1237000 Btu/h ft²).

[Video 1.11.3](#) and [video 1.11.4](#) (slow motion): *CHF in an Annulus (2nd run)*. The videos display CHF occurring at the following test conditions: inlet temperature is 25°C (77°F), outlet temperature is 29°C (84.2°F), outlet pressure is 3 bar (43.5 psia), inlet subcooling is 110 K (198°F), mass velocity is 3250 kg/m²s (2390000 lb/hft²) and liquid velocity is 3.3 m/s (10.8 ft/s). The heat flux of CHF in this video was 9400 kW/m² (2980000 Btu/h ft²).

[Video 1.11.5](#) and [video 1.11.6](#) (slow motion): *CHF in an Annulus (3rd run)*. The videos display CHF occurring at the following test conditions: inlet temperature is 22°C (71.6°F), outlet temperature is 27°C (80.6°F), outlet pressure is 1.1 bar (16 psia), inlet subcooling is 165 K (297°F), mass velocity is 7550 kg/m²s (5550000 lb/hft²) and liquid velocity is 7.5 m/s (24.6 ft/s). The heat flux of CHF in this video was 12700 kW/m² (4027000 Btu/h ft²).

1.12 FLASHING IN TUBES

Flashing is an important two-phase flow phenomenon. Flashing for example can occur when a liquid is suddenly reduced far below its saturation pressure without the immediate occurrence of boiling. For instance, flashing of a saturated or near saturated liquid may occur when passing through a nozzle, an expansion device or from a small to a larger channel. As a result, the liquid becomes superheated and thus unstable. The phenomenon is characterized by very rapid evaporation, which occurs in the videos below as a wave-like evaporation process, which in some cases may even have an adverse effect on the integrity of the system and safety.

The videos below display flashing of dodecane inside a vertical glass tube of 15 mm (0.59 in.) internal diameter. The tests were done with the glass tube filled with liquid dodecane separated from the low pressure reservoir by its own saturated vapor and a diaphragm. The experiments were done in an upright position so that the top of the tube corresponds to the right side of the images (initially the liquid is below its own high pressure vapor and the diaphragm that separates it from the low pressure reservoir). Each experiment started by piercing the diaphragm exposing the liquid and vapor to the low-pressure environment. In the video, the interface between the saturated liquid and its high pressure vapor is seen at the beginning before the thin diaphragm (which is not visible in the video) is burst. The evaporation wave moves from top to bottom. The videos were taken at 3000 images per second and are shown here in slow motion. The videos were taken by José Simões-Moreira during his Ph.D. in the laboratory of Prof. J.E. Shepherd at CalTech. The test setup and results are described in Simões-Moreira and Shepherd (1999) and in the Ph.D. thesis at RPI of Simões-Moreira (1994). José Simões-Moreira is presently a professor at the University of San Paolo in San Paolo, Brazil.

List of videos: (click on the one you wish to see)

[Video 1.12.1](#): *Flashing in a vertical tube (1st run)*. The 1st run is for an initial saturation temperature of the dodecane at 200°C (392°F) while the low pressure reservoir is at an initial pressure of 1 mbar absolute (0.015 psia), i.e. nearly at vacuum.

Video 1.12.2: *Flashing in a vertical tube (2nd run)*. The 2nd run is for an initial temperature of the dodecane of 250°C (482°F) while the low pressure reservoir is at an initial pressure of 1 mbar absolute (0.015 psia).

Video 1.12.3: *Flashing in a vertical tube (3rd run)*. The 3rd run is for an initial temperature of the dodecane of 250°C (482°F) while the low pressure reservoir is at a higher initial pressure of 0.75 bar absolute (10.9 psia).

1.13 TWO-PHASE FLOWS IN PLATE HEAT EXCHANGERS

Plate heat exchangers are an important type of two-phase heat exchanger used for both evaporation and condensation, especially in small to medium size refrigeration applications. Very few two-phase flow videos are available for flow between the plates. Presently, three distinct types of plates are illustrated in the videos. All tests were for R-134a with adiabatic upward flow at a saturation temperature of 10°C (50°F). In their videos, the vapor quality is denoted as “X” in %, the mass velocity is denoted as “G” in kg/m²s, “C” refers to Chevron plates, “LB” refers to long bump plates and “RB” refers to round bump plates. The nine videos below were taken by E.W. Jassim during his M.S. in the laboratory of Profs. T.A. Newell and J.C. Chato at the Air Conditioning and Refrigeration Center at the Department of Mechanical and Industrial Engineering at the University of Illinois at Urbana-Champaign. Only their videos at low vapor qualities are shown here. The test setup and results are described in Jassim, Newell and Chato (2006) and Jassim (2000). For detailed descriptions of the plates and their dimensions, refer to their publications.

List of videos: (click on the one you wish to see)

Video 1.13.1: *Two-phase flow in a chevron plate heat exchanger (1st run)*. The 1st run is for a mass velocity of 60 kg/m²s (44100 lb/hft²) over the vapor quality range from 5 to 7%.

Video 1.13.2: *Two-phase flow in a chevron plate heat exchanger (2nd run)*. The 2nd run is for a mass velocity of 90 kg/m²s (66200 lb/hft²) over the vapor quality range from 5 to 7%.

Video 1.13.3: *Two-phase flow in a chevron plate heat exchanger (3rd run)*. The 3rd run is for a mass velocity of 125 kg/m²s (92000 lb/hft²) over the vapor quality range from 5 to 7%.

Video 1.13.4: *Two-phase flow in a long bump plate heat exchanger (1st run)*. The 1st run is for a mass velocity of 60 kg/m²s (44100 lb/hft²) over the vapor quality range from 5 to 7%.

Video 1.13.5: *Two-phase flow in a long bump plate heat exchanger (2nd run)*. The 2nd run is for a mass velocity of 90 kg/m²s (66200 lb/hft²) over the vapor quality range from 5 to 7%.

Video 1.13.6: *Two-phase flow in a long bump plate heat exchanger (3rd run)*. The 3rd run is for a mass velocity of 125 kg/m²s (92000 lb/hft²) over the vapor quality range from 5 to 7%.

Video 1.13.7: *Two-phase flow in a round bump plate heat exchanger (1st run)*. The 1st run is for a mass velocity of 60 kg/m²s (44100 lb/hft²) over the vapor quality range from 5 to 7%.

Video 1.13.8: *Two-phase flow in a round bump plate heat exchanger (2nd run)*. The 2nd run is for a mass velocity of 90 kg/m²s (66200 lb/hft²) over the vapor quality range from 5 to 10%.

[Video 1.13.9](#): *Two-phase flow in a round bump plate heat exchanger (3rd run)*. The 3rd run is for a mass velocity of 125 kg/m²s (92000 lb/hft²) over the vapor quality range from 5 to 7%.